An image analysis method for quantifying precision and disorder in nanofabricated photonic structures

Henry S. Carfagno¹, P. D. García², Matthew F. Doty¹

 $^{\rm 1}$ Dept. of Materials Science and Engineering, University of Delaware, $^{\rm 2}$ Instituto de Ciencia de Materiales de Madrid

E-mail: carfagno@udel.edu

Abstract. Disorder is an essential parameter in photonic systems and devices, influencing phenomena such as the robustness of topological photonic states and the Anderson localization of modes in waveguides. We develop and demonstrate a method for both analyzing and visualizing positional, size, and shape disorder in periodic structures such as photonic crystals. This analysis method shows selectivity for disorder type and sensitivity to disorder down to less than 1%. We show that the method can be applied to more complex shapes such as those used in topological photonics. The method provides a powerful tool for process development and quality control, including analyzing the precision of E-Beam Lithography before patterns are transferred; quantifying the precision limits of lithography, deposition, or etch processes; and studying the intentional displacement of individual objects within otherwise periodic arrays.

Submitted to: Nanotechnology

1. Introduction

E-beam lithography (EBL) tools can now routinely write features smaller than 10 nm and device features on these length scales are becoming increasingly important for photonic devices [1] Fabrication precision is extremely important for device performance because small deviations from ideal designs can introduce scattering sites that leads to significant loss and interference spoiling the optical performance. [2–4] For example, Dario Gerace and Lucio Claudio Andreani develop a sophisticated computational model of the sensitivity of the performance of photonic crystal devices on the disorder present. They report an exponential decrease in the performance of photonic crystal cavities and waveguides as a function of a linear increase in disorder. [3] The results of Gerace suggest that disorder larger than a few percent will lead to unacceptable decreases in device performance. This result sets an approximate bound on the amount of disorder that can be tolerated within photonic crystal-like devices. As a possible solution to this bottleneck, topological photonics can provide robust protection against fabrication defects, but only if the uniformity of the fabricated structures is below fluctuations within the nanometer scale, although this value depends strongly on the group index of the transmitted light. [5] However, disorder and intentional variation can also be exploited to enhance light-matter interactions in nanophotonic and quantum optic devices. [6] For example, small changes in the diameter or position of holes near the boundaries of photonic crystal cavities can significantly alter the cavity quality factor (Q).[7] Similarly, small intentional variations in the position or size of a hole on the boundary of a photonic crystal waveguide can be used to create Anderson localized photonic modes. [8] For all of these reasons it is becoming increasingly important to be able to measure the precision limits of lithography and fabrication steps and to know the precision with which intentional variations in feature size or position can be realized in a device.

Scanning Electron Microscopy (SEM) is the most common tool used for monitoring and evaluating photonic devices with nm-scale features during process development and implementation. Absolute measurements of the size of individual features patterned by EBL or transferred via deposition or etch cannot be directly extracted from SEM images because the apparent size of a feature can be easily distorted by the contrast and focusing of the SEM; this imaging uncertainty convolves with any imperfections in the EBL mask write or any subsequent pattern transfer. However, any such distortions will be applied equally to all elements of an image. Although important progress has been made to quantify disorder applying statistical analysis of scanning electron micrographs, [9] the reconstruction of actual dielectric profiles from scanning electron microscopy is not straightforward. [10] A possible solution to this involves using optical far-field measurements, [2] but this technique requires a rather advanced optical setup. Here, we present an SEM image analysis method that allows us to quantify the precision limits of an EBL process and a subsequent inductively coupled plasma reactive ion etch (ICP RIE) transfer of the EBL mask. Specifically, we take advantage of the uniformity of periodic structures such as the array of holes in a photonic crystal to obtain precise measurements of the disorder of individual elements relative to the mean. We started by creating patterns with varying degrees and types of intentionally-induced disorder. We obtained SEM images of all of these samples and applied a custom-developed image analysis protocol to analyze and quantify the degree and type of disorder in the SEM images. From this data, we determine the precision limits of our measurement. We then show how this method can be applied to characterize photonic devices by measuring the precision with which we can realize a) a topological photonic pattern and b) intentionally-induced displacements of individual holes in a photonic crystal array. A particular advantage of this approach, as we will show, is the capacity to compare, via SEM, the effect of varying process parameters on the resulting sample quality. The method also provides an important quality-control tool that can save time by identifying insufficient sample quality (e.g. after a mask write) before subsequent process steps are implemented.

2. Methods

2.1. Summary of Approach

Our goal was to develop image analysis methods that can be applied to any photonic devices based on two-dimensional arrays of repeated elements. Our test case for developing this method comprised 1) a GaAs heterostructure with typical parameters for a suspended membrane photonic crystal device and 2) hexagonal-array photonic structures with both circular and shamrock unit cells. All measures of disorder will be reported as a percentage of the hexagonal lattice constant (%) or as a length (nm). We start by focusing on positional and size (radial) disorder for a hexagonal array of circles - a standard photonic crystal design. Positional displacements Δx , Δy , and Δxy are the displacement of a unit cell from its proper lattice position along the x, y, and combined x and y directions, respectively. Likewise, radial distortions Δr_x and Δr_y are the difference between the radius of an individual circular element along the x and y directions, respectively, relative to the mean radius. Unequal Δr_x and Δr_y indicate ellipticity, which could be introduced intentionally or unintentionally. For clarity, we will use the term "measured-disorder" in a statistical sense. For example, an analysis of N unit cells returns a histogram of N measured values of Δx that follows a normal distribution with a standard deviation δx . δx is the measured-disorder we report. We note that this measured-disorder is not strictly equivalent to "actual-disorder" because what we can measure necessarily convolves the actual-disorder in the sample (i.e. the limits of fabrication) with the limits of SEM accuracy and the choices made during the analysis protocol. As we will show, our image analysis protocol provides a powerful tool for improving the rigor with which SEM images can be analyzed for process optimization and sample qualification despite this limitation.

The image analysis protocol starts by processing an SEM image of a given sample,

as shown in Fig. 1. First, the image is smoothed to reduce pixelated noise. Second, a brightness cutoff level is chosen to produce a Boolean black/white mapping. The choice of this cutoff level and the brightness and contrast levels used in the capture of the SEM image are the primary limitations on the accuracy of reported values such as radius. Precision, which derives from comparison of measurements of one element to the mean, is not affected by these limitations. Using the Boolean mapping, pixels are grouped into objects. The largest area, which is mostly the contiguous background, and all small objects are removed. This choice assumes an actual-disorder in unit cell area below a threshold, which is a safe assumption because actual-disorder above this threshold would be easily seen by simple visual inspection of the SEM image. Pixels which are strictly interior to the remaining objects and assigned as bright during the boolean mapping are flipped. For circles the perimeter is smoothed by averaging over a few nearest-neighbor pixels. Finally, we evaluate the resulting objects for metrics such as centroid positional measured-disorder and radial measured-disorder. Information about the software we wrote to implement this method, and links to download it for adaptation and re-use, are provided in the supplemental information.

2.2. Sample fabrication

The sample mask files were generated using the NIST nanolithography toolbox. Masks consisted of hexagonal photonic crystals with a lattice constant of 500nm and radius of 150nm. These parameters target photonic structures centered on 1550nm, a standard telecom wavelength, given a membrane thickness of 145nm. To test the image analysis approach, the EBL mask files included intentionally added disorder of various types ranging from 0% to 6% in 0.5% intervals. For example, to achieve 2% intentionally added x-position disorder, the center position of each circular feature, in the mask file, was displaced in the x-direction by a random value chosen from a normal distribution with a 2% standard deviation.

All samples start with a bare GaAs substrate. A resist mask, AR-P6200.09, is spun onto the surface at 3000 RPM for 60s. The sample is then baked on a hot plate at 170C for 5:00 minutes. The sample backside is cleaned with NMP. The sample is dosed in our EBL system (Raith EBPG5200ES) to 200 uC/cm² using a beam current of 1nA. Resist development is done with AR600-546 for 120s under slight agitation. An oxygen asher plasma is then used to clean residuals in the features. Samples in which the resist mask is imaged are imaged after the asher plasma clean. Etched samples are not exposed to the electron beam in the SEM before they are etched via a Chlorine based Inductively Coupled Plasma (Cl-ICP) etch. The BCl₃ and Ar gas flowrates for this etch are 15sccm and 10sccm, respectively, and the coil power and bias power are 500W and 25W, respectively. The etch time was 160 seconds and the chamber pressure was 6mTorr. The resist is then removed by a 2hr soak in NMP followed by a 15min sonication, before the etched features are imaged in the SEM.

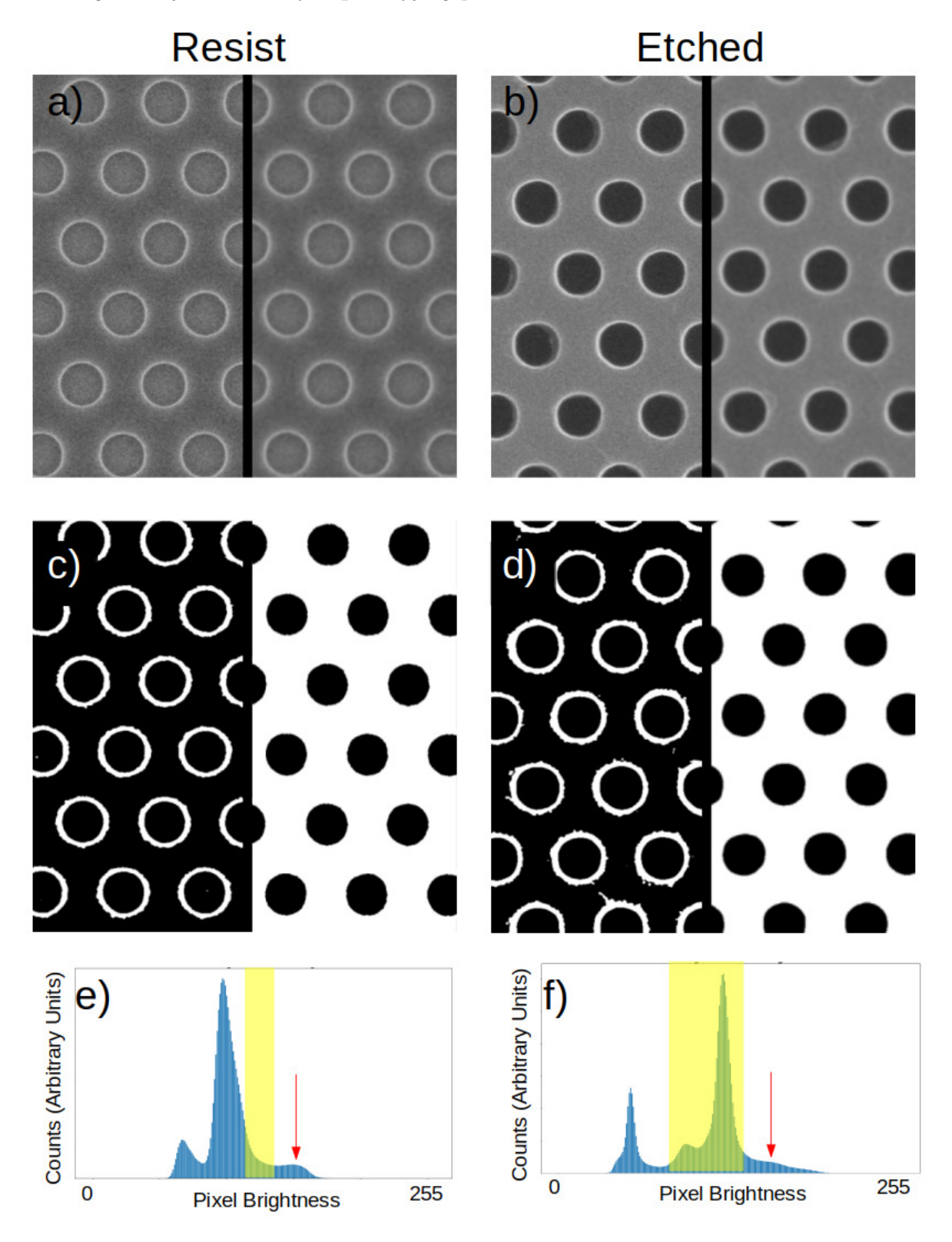


Figure 1. Image analysis on resist mask (a, c, e) and etched sample (b, d, f). a, b) the original (left side) and smoothed (right side) SEM images. c, d) the Boolean mapping of the smoothed image (left) and after the background is removed (right). e, f) Pixel brightness histograms for the smoothed SEM images. The red arrow points to the peak associated with the bright edges of each circular feature. The range of brightness cutoff levels that can be used to generate the Boolean mappings in (c, d) are highlighted in yellow.

2.3. SEM imaging

SEM image quality has a direct impact on the disorder that can be measured in a given image, and many image acquisition parameters are important. For example, magnification and image resolution together determine actual pixel size in nm. High image resolution allows for a small pixel size while maintaining a field of view large enough to include enough unit cells for a statistically relevant calculation of measured-disorder. Scan speed, image resolution, and frame/line averaging impact acquisition time. Long acquisition time can produce image drift from beginning to end, which can be compensated somewhat with drift-compensated frame averaging. For the majority of the results presented in this paper, the image resolution was 4096 by 3072 pixels. A magnification was chosen such that 400 unit cells were in the field of view. This resolution and magnification resulted in a pixel size of approximately 3.5nm. A scan speed was chosen such that a frame was captured in under 2 seconds. Drift compensated frame averaging was used to reduce signal to noise and resulted in a total acquisition time of about 2 minutes per image.

2.4. Image Analysis

The first step in the image analysis is to smooth the image, which produces a significant improvement in signal to noise at the cost of absolute image accuracy. We smoothed our image by averaging nearest neighbors and layering (repeating) this averaging 4 times. The results of this smoothing can be seen in Fig. 1a for a resist mask sample, where the original SEM image is on the left side of the panel and the smoothed image is on the right side of the panel. Similarly for the etched sample in Fig. 1b. It is clear from Fig. 1a and b that the objects in the image (the circular holes) are large enough to be largely unaffected by this pixel-level smoothing. Thus, for a radially-symmetric object this smoothing should have vanishingly-little impact on the centroid position and only marginal impact on the radial displacement relative to the group's average.

In the second step the gray-scale image is converted into a black / white image by conducting a Boolean mapping with a simple brightness level cutoff that determines which pixels are mapped to white vs. black (1 vs. 0 in the digital image file). Fig. 1e and f show the pixel brightness histograms for the smoothed SEM images (Fig. 1a and b). The results of the Boolean mapping are shown on the left side of Fig. 1c and d, where the brightest features (the edges of the holes) are mapped to white and the relatively dark features and background are mapped to black. The specific brightness cutoff value can be selected from anywhere in the range highlighted in yellow in Fig. 1e and f, which guarantees that the pixels associated with the brightness (edge) features (indicated by the red arrow) map to white. We note that the brightness cutoff level is the only choice the user has to make and the pixel brightness histograms show how quantitative and robust this choice can be. In the third step, the background (the largest contiguous object) is flipped from black to white. Noise in the image can result in very small features in the region between the bright edge and the nominally dark background and

these are also flipped to white if they are less than 20% the size of the largest circular feature (i.e. far too small to be due to feature size disorder). Any white pixels interior to each circular object are flipped to black, again eliminating effects of noise. In the fourth step, the edges of each circular object are smoothed by expressing the perimeter in polar coordinates and applying a Fourier filter eliminating noise with a spatial period shorter than a couple of pixels. We did not apply this smoothing procedure to shamrock features (see below), only to circular features for which distortions of the feature shape due to this filtering should be negligible. The end result of these image manipulation steps is a black and white image in which each feature is a contiguous black solid without voids and in which the background is uniformly white, i.e. the images on the right side of Fig. 1c and d.

In the final step we analyze the image to extract the relevant information. Our software first calculates the centroid of each object, which gives its location. We use the values of the centroids for each object to define the coordinate basis for the overall hexagonal lattice and can then compute the displacement of each individual feature (e.g. Δx , Δy) relative to the perfect position defined by the lattice. The area of each object is used to compute a circularized radius, from which we can compute the measured variation in the isotropic radius of each feature relative to the mean. The radius in the x-direction (Δr_x) can be computed by the average distance from the centroid to the edge in a $2\pi/10$ radian window around the x axis. Similarly for Δr_y . The ellipticity and major axis alignment can be directly calculated from the object boundry. Each of these calculations is done individually for all the objects in the field of view, resulting in a distribution of values for each parameter from which a standard deviation is calculated to obtain the measured-disorder for each parameter (i.e. δx).

3. Sensitivity and Precision Analysis

3.1. Measurements of Resist-only vs Etched Samples: effective noise floor

We assess the effective noise floor of our image analysis protocol by quantifying all types of measured-disorder as a function of the intentional disorder of a specific type added to the mask files of each sample. By effective noise floor we mean the lowest disorder that can be reliably measured using the reported method. We determine this effective noise floor by defining, fabricating, and imaging samples with zero intentional disorder. For example, Fig. 2 shows the measured-disorder as a function of the amount of intentionally-added x-position disorder for both resist-only (a) and etched (b) samples. We emphasize that each intentional x-position disorder value along the x axis of the figures corresponds to an individual sample that was fabricated and imaged and for which measured disorder values for δx , δy , δr_x and δr_y were obtained. We focus first on the measured- δx -disorder. In both cases (resist and etched samples), we expect the measured- δx -disorder to roughly follow the 1:1 reference line (blue). Good agreement with the 1:1 reference is seen for higher intentional and measured-disorders, but the

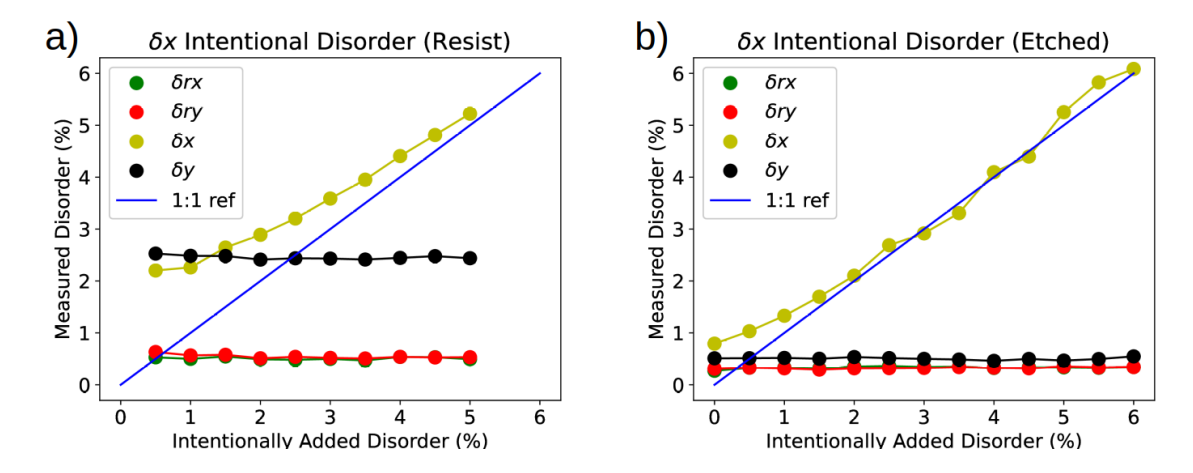


Figure 2. Measured-disorder vs. intentionally added disorder for a) resist samples, and b) etched masks. The difficulty in imaging resist shows in the higher background and lower sensitivity.

measured-disorder deviates from the 1:1 reference and asymptotes toward 1.5% (2.5%) for lower intentionally-induced disorder in the etched (resist) sample. This asymptotic limit is the noise-floor of our method - the lowest level of measured-disorder that can be reliably extracted from our image analysis method.

The noise-floor is due to a combination of the precision limits associated with the EBL mask fabrication, the SEM image acquisition, and this image analysis method. The lower effective noise floor for the etched sample is a consequence of the better contrast in the original SEM images, which can be seen clearly by comparing the left and right columns of Fig. 1 that show the progression of the image analysis technique for resist mask and etched samples, respectively. The reduced contrast for the resist-only samples is partially a result of the fact that the resist tends to shrink under exposure to the electron beam of the SEM, ruining the resist profile and resulting in a poor image. In contrast, the bare GaAs is largely unaffected by the electron beam and thus a higher beam current can be used for a longer time, allowing for the SEM images with good contrast. The remainder of our discussion will focus on analysis of images of etched samples. We stress, however, that Fig. 2a demonstrates that imaging and analysis of resist-patterned samples, without etching, can be used to determine whether or not an EBL process is achieving precision at least as good as the effective noise floor.

3.2. Selectivity in Disorder Type

We now consider the sensitivity to different types of disorder. Fig. 2 shows that δy , δr_x and δr_y are all relatively constant regardless of the magnitude of the intentionally-added δx disorder. These data demonstrate that this method has good selectivity in discriminating which type of disorder is present in the sample. We next conducted similar tests for all of the possible disorder parameters. The results can be seen in Fig. 3. In Fig. 3a the y-position of the circular holes is intentionally varied and imaged

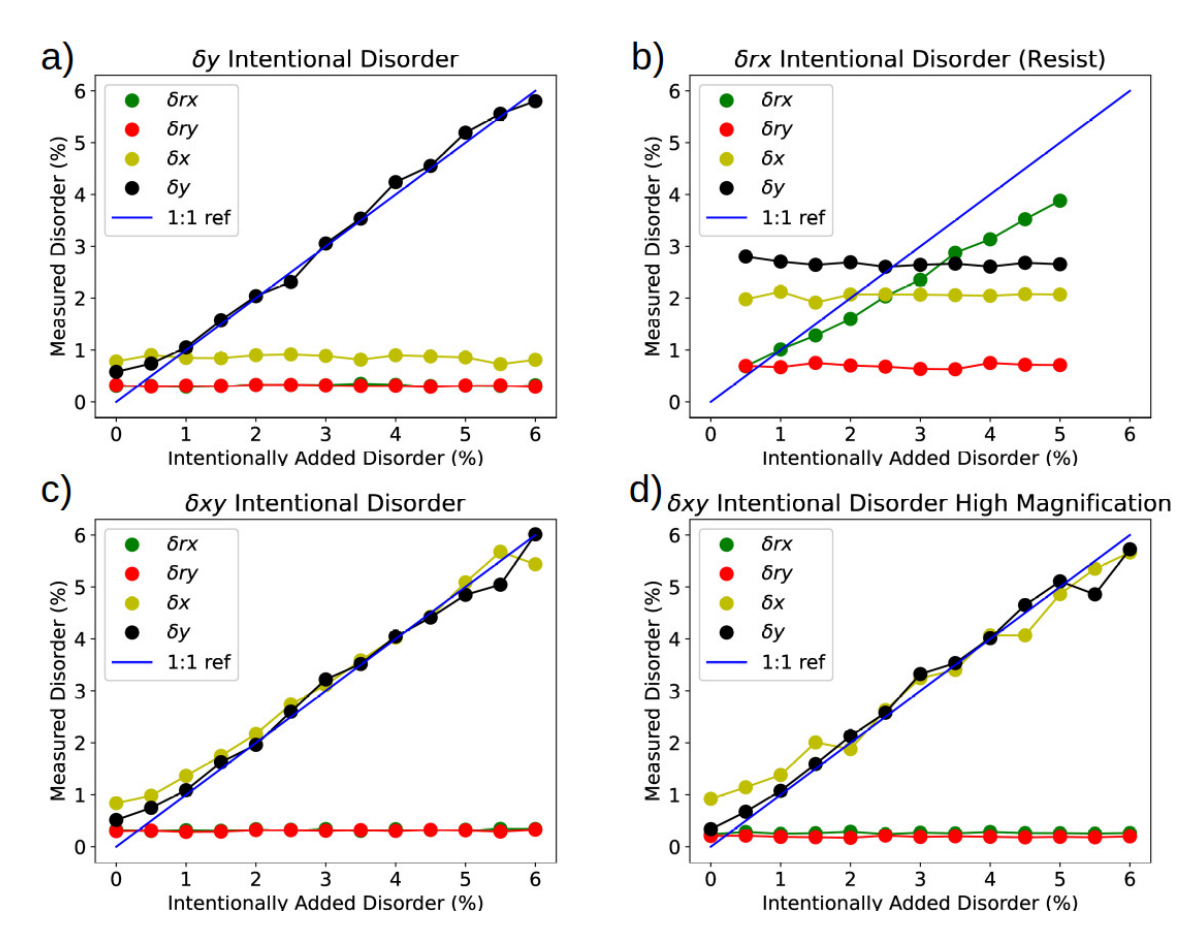


Figure 3. Analysis of a) dx type disorder, b) dy type disorder, c) dxy type disorder, d) dxy type disorder with a higher magnification SEM setting such that the pixel size is 1.5nm which is smaller than the pixel size of 3.5nm in c). Note that for each test the only measured-disorder(s) that tracks the 1:1 reference line are the disorder(s) intentionally added. Note that the other disorder types appear largely flat. These two observations together show excellent selectivity toward disorder types. Note in b) that the analysis was conducted on a resist-mask demonstrating the analysis' usefulness at varying process steps.

an etched samples. In Fig. 3b the radius of the holes is intentionally varied and imaged in a resist-mask samples. In Fig. 3c and d both the x- and y-positions of the circular holes are intentionally varied. In each case the data show that the image analysis methods is selective in the type of disorder present. The measured-disorder for nominally-fixed parameters remains constant, typically at or below 1% measured-disorder. The measured-disorder for the intentionally-varied parameter tracks the expected 1:1 line above the effective noise floor, which is also $\sim 1\%$. These data demonstrate that the image analysis method can selectively probe different types of disorder and distinguish between them.

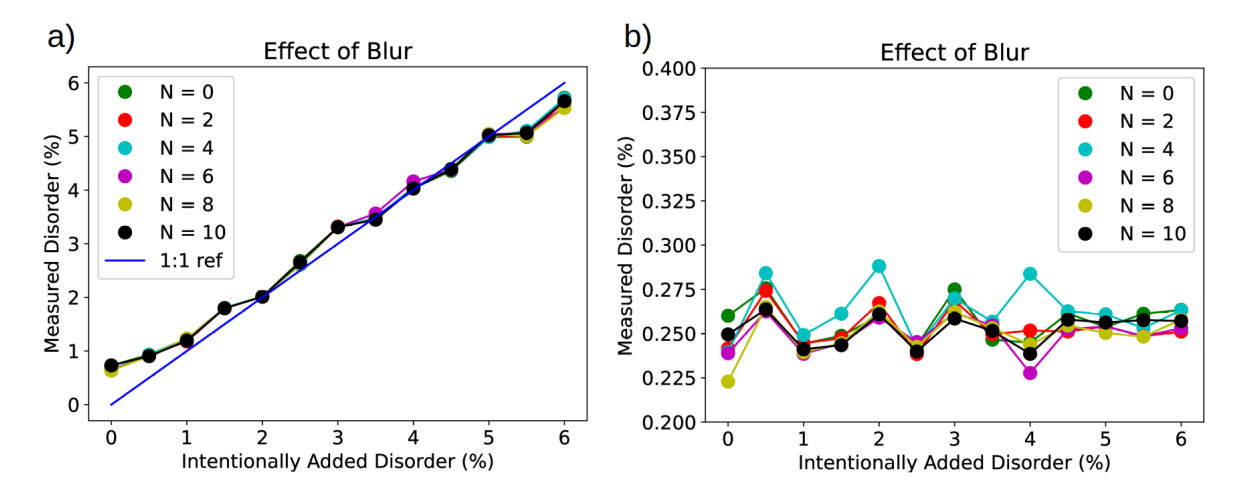


Figure 4. Analysis of high magnification SEM images of samples with intentional δxy disorder demonstrates that the number of smoothing iterations does not significantly alter the precision limits. Neither a) the measured intentional δxy disorder nor b) the measured δrx (not intentionally varied) depend, within the noise limits, on the number of smoothing iterations.

3.3. Impact of image acquisition and analysis parameters

We next consider the effect of image acquisition and analysis parameters on the measured-disorder returned using this method. We start by considering the effect of SEM magnification. Higher magnification decreases pixel size, which allows for a more accurate SEM image. However, we find that increased magnification does not improve the accuracy of the measurement and may even reduce accuracy. See Fig. 3c and d, which analyze the same series of samples using normal (c) and higher-magnification (d) SEM images. Fig. 3d shows no significant improvement in the effective noise floor and a slight increase in the deviation from the 1:1 reference line for higher intentional disorders. We believe that while increasing the magnification improves the pixel size and SEM accuracy, this gain comes at the expense of a reduced number of unit cells in the image. We conclude that increased magnification does not improve our measurements because the reduction in the number of unit cells in the sample image has a more significant (negative) impact on the overall measurement precision.

We next analyze whether the variations in the number of image smoothing iterations alters the precision or effective noise floor of this method. Fig. 4a presents the measured δxy disorder as a function of intentionally-introduced δxy disorder for images processed with varying number of image smoothing iterations. If the image smoothing were degrading the precision of the measured-disorder, we would expect to see a higher effective noise floor for higher numbers of smoothing iterations because images processed with, say, 10 smoothing iterations are averaging over a 10x larger spatial area. Fig. 4a shows that the number of smoothing iterations has no appreciable affect on the results of the measured-disorder for δxy . In Fig. 4b we present a similar analysis that shows that the number of smoothing iterations has a negligible effect on measured δrx disorder,

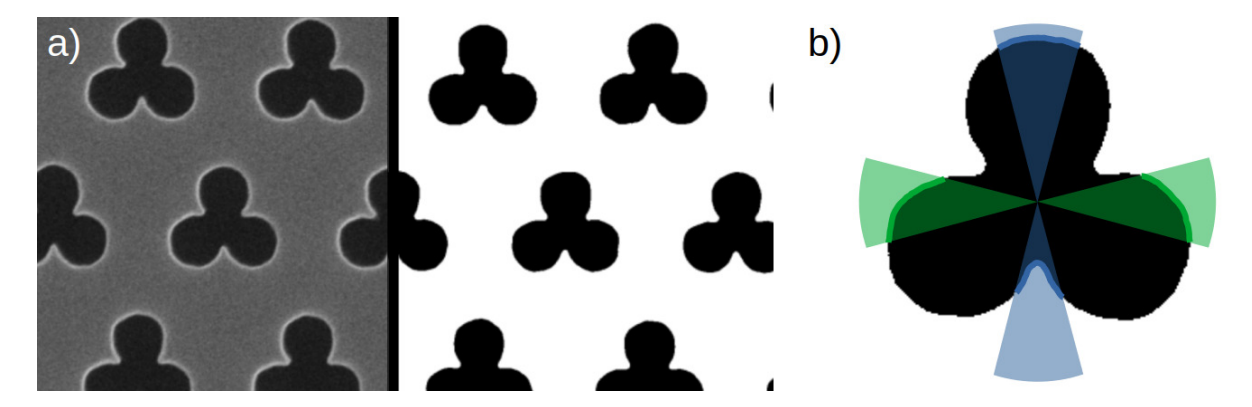


Figure 5. Analysis of topological photonic crystal. a) Original SEM (left) and Boolean mapped (right) images of the fabricated sample. b) r_x (green) and r_y (blue) are defined to be half the average cross section of the feature taken through the centroid in an arc of 0.2π rad centered on the x and y axes, respectively. δr_x and δr_y are thus the standard deviation of a well-defined size and shape parameter across the ensemble of shamrock features.

which was not intentionally varied for this sample. This further confirms that the effective noise floor is not significantly altered by the number of smoothing iterations.

3.4. Precision

To quantify the precision of our protocol for extracting measured disorder we can perform a statistical analysis on the data. Consider the δxy case in Fig. 4 with zero blurring steps, which has 13 data points. A simple linear fit to these 13 data points has a slope (sensitivity) of 0.86. The average deviation of these 13 data points from this fit is 0.1476%. Using a t-distribution we compute from this data a 95% confidence interval of 0.3188%. Using this 95% confidence interval and the measured sensitivity (0.86), we conclude that the 95% confidence interval for measuring some actual disorder is around 0.3705%. In other words, this method could distinguish, with 95% confidence, between any two samples with a difference in disorder of at least 0.741%. This provides a powerful tool for comparing, for example, which fabrication process conditions transfer a pattern with maximum fidelity.

4. Example Applications

The approach we develop and present can be generalized to characterize any twodimensional regular array of features. One the left side of Fig. 5a we show an SEM image of a photonic crystal device we fabricated with "shamrock" shaped holes that break symmetry and enable topological photonic states. The Boolean map of this SEM image, shown on the right side of Fig. 5a, demonstrates that the image analysis algorithm is able to identify the shamrock shape, all perimeter points, and all interior points, from which it can calculate the centroid of each unit cell. As reported in Fig. 5b, the image analysis algorithm is able to compute measured-disorder values for δx , δy , δr_x and δr_y

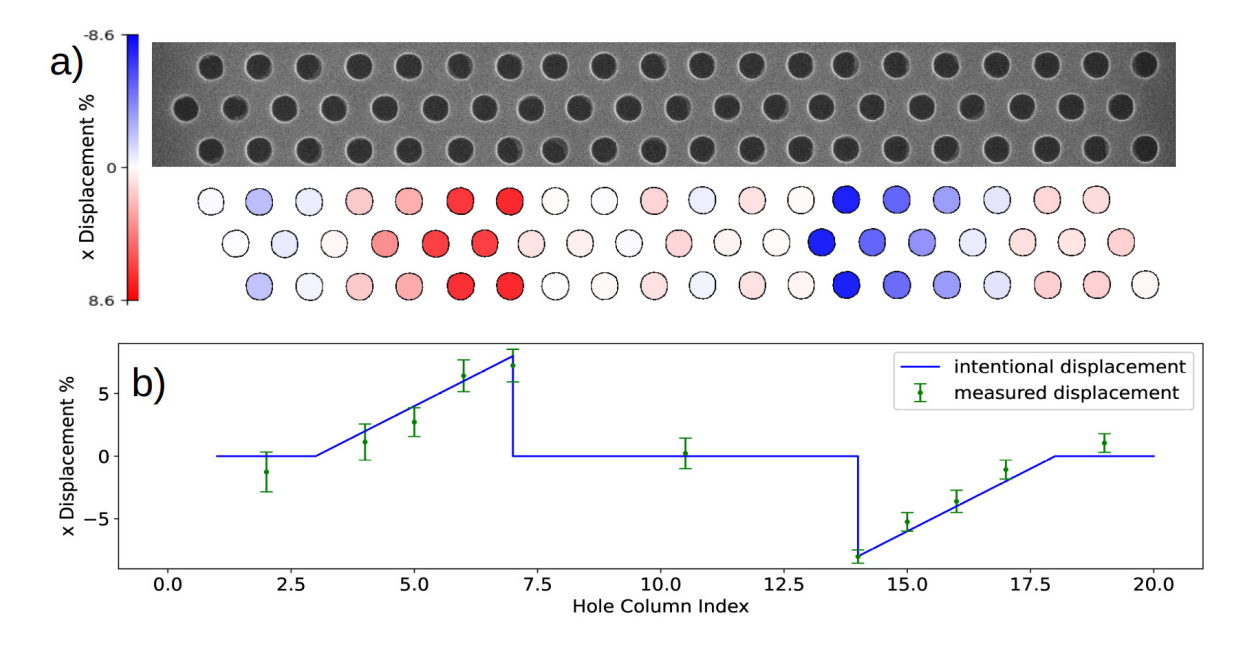


Figure 6. Color mapped x-position disorder of sample including localized intentional x-position disorder.

values. The measured-disorder values for δx and δy are 1.0% and 0.8%, respectively. Because these values are below the effective noise floor determined through our analysis above we conclude that the measured x and y positional disorder of the centroid of each shamrock unit cell relative to the desired lattice is no larger than our effective noise floor of 1.5%.

Characterizing size and shape disorder in complex features such as shamrocks is somewhat more complicated, but still possible with this image analysis method. For shamrock-shaped features, Δr_x and Δr_y correspond to half the distance between opposite sides of the feature perimeter along a cross section passing through the centroid and averaged over an arc of $2\pi/10$ radians about the x or y axis, respectively, as depicted in Fig. 5b. While these values have no particular geometric significance for shamrocks, they provide a useful measure of pattern transfer fidelity. For example, a cross section along the y axis of a shamrock, as shown in Fig. 5a, should be significantly reduced by the upward-pointing \wedge between the lower-left and lower-right "leaves." If etch conditions are significantly altering the placement of this \wedge or its extent along the y axis, this would be captured by changes in Δr_{ν} . Similarly, inconsistencies in the size or placement of this \wedge between individual shamrocks would result in increased δr_y . We find the measureddisorder for both δr_x and δr_y is 0.3%, again below the effective noise floor and indicating that the size and shape uniformity of the fabricated shamrocks is no worse than 1.5%. We emphasize that the method reported here calculates the perimeter and position of every imaged object. From this data, any geometric parameter involving the shape and position of arbitrarily-shaped topological objects could be calculated and statistically evaluated.

We next demonstrate that this image analysis method can be used to visualize

both intentional and unintentional disorder or offsets. In Fig. 6 we report the analysis of a sample fabricated with varying intentional spatial offsets along the x direction for individual circular features. The top of Fig. 6a shows the SEM image of the fabricated sample, and we note that simple visual inspection of this SEM image suggests it is a perfectly periodic structure. The lateral offset in hole position that was included in the mask file for individual columns of holes is shown by the solid blue line in Fig. 6b. The bottom of Fig. 6a shows shows a visualization output from our image analysis method in which the color (red - white - blue) indicates the x-direction displacement (positive - zero - negative) of each individual hole relative to the lattice. The data points in Fig. 6b show the measured average values of x-direction displacement, relative to the lattice, for the holes within each column. The excellent agreement between the displacement included in the mask file (solid line) and that measured by the image analysis (points) provides further validation of the precision with which this method can determine feature positions. More importantly, the image analysis performed to obtain Fig. 6b does not utilize any prior knowledge of the intended lateral displacements. Indeed, the measured displacements of features in the regions with zero intentional lateral displacement (center and outside edges of Fig. 6b) demonstrates the capacity of this method to measure and visualize unintentional displacements of features within twodimensional arrays. Similar methods could be used to visualize unintentional variations in feature perimeter, ellipticity, or perimeter.

Finally, we reiterate that this image analysis method provides a powerful tool for process development and troubleshooting. For example, a visualization such as that presented in Fig. 6 could be used to understand systemic disorder originating from EBL write errors such as write-field alignment, drift, or the proximity effect. Similarly, such an analysis could be used to evaluate the fidelity with which increasingly complex feature shapes (e.g. shamrocks) are realized as a function of varying process conditions such as single- vs. multi-pass EBL or varying ICP etch parameters. Perhaps most importantly, this image analysis method provides a quality-control tool that allows one to qualify process conditions without relying solely on photonic performance of completed devices and to reject samples that do not meet quality or uniformity metrics before subsequent process steps are implemented.

5. Conclusion

We present a SEM image analysis method for characterizing disorder in two-dimensional arrays of features such as those routinely used in photonic crystals. We demonstrate that the method is selective to different types of disorder and is sensitive to intentionally-added disorder down to $\sim 1\%$. While other much more demanding methods[2] that rely on far-field optical measurements can quantify disorder down to 0.005 %, our method is able to discriminate different types of disorder, something that is not possible with optical measurements. Furthermore, we demonstrate that this method can be applied to more complex unit cell shapes such as those used in phononics,[11] and be used to

REFERENCES 14

measure and visualize both intentional and unintentional disorder. We expect that this method will provide a powerful tool for the development of fabrication methods for realizing increasingly complex photonic components such as those that offer topological protection or localization of modes at lattice defects such as displaced or differently-sized features.

6. Acknowledgements

This research was primarily supported by NSF through ENG-1839056. This research was partially supported by NSF through the University of Delaware Materials Research Science and Engineering Center, DMR-2011824.

References

- [1] Albrechtsen M, Lahijani B V, Christiansen R, Nguyen V, Casses L, Hansen S, Stenger N, Sigmund O, Jansen H, Moerk J and Stobbe S 2021 URL http://dx.doi.org/10.21203/rs.3.rs-738060/v1
- [2] García P D, Javadi A, Thyrrestrup H and Lodahl P 2013 Applied Physics Letters 102 031101
- [3] Gerace D and Andreani L C 2005 Photonics and Nanostructures Fundamentals and Applications 3 120-128 ISSN 1569-4410 the Sixth International Symposium on Photonic and Electromagnetic Crystal Structures (PECS-VI) URL https://www.sciencedirect.com/science/article/pii/S1569441005000271
- [4] Minkov Μ, Dharanipathy U Ρ, Houdré R and Savona V 2013 Opt.Express21 28233-28245 URL https://opg.optica.org/oe/abstract.cfm?URI=oe-21-23-28233
- [5] Arregui G, Gomis-Bresco J, Sotomayor-Torres C M and Garcia P D 2021 Quantifying the robustness of topological slow light URL http://dx.doi.org/10.1103/PhysRevLett.126.027403
- [6] García P D and Lodahl P 2017 Annalen der Physik 529 1600351
- [7] Akahane Y, Asano T, Song B S and Noda S 2003 Nature 425 944–947
- [8] Topolancik J, Ilic B and Vollmer F 2007 Experimental observation of strong photon localization in disordered photonic crystal waveguides URL http://dx.doi.org/10.1103/PhysRevLett.99.253901
- [9] Le Thomas N, Diao Z, Zhang H and Houdré R 2011 Statistical analysis of subnanometer residual disorder in photonic crystal waveguides: Correlation between slow light properties and structural properties URL http://dx.doi.org/10.1116/1.3622289
- [10] Skorobogatiy M, Bégin G and Talneau A 2005 Opt. Express 13 2487-2502 URL http://opg.optica.org/oe/abstract.cfm?URI=oe-13-7-2487

REFERENCES 15

Arregui Ng С, [11] Florez Ο, G, Albrechtsen Μ, R Gomis-Bresco D Sotomayor-Torres and García J, Stobbe S, \mathbf{C} Μ Ρ URL https://arxiv.org/abs/2202.02166

7. Supplemental Material

7.1. Image analysis Code information and GitHub link

https://github.com/anonymized 861674/Image-Analysis